

A Quantum Dynamics Study of the Hyperfluorescence Mechanism: Supporting Information.

Yvelin Giret, Julien Eng, Thomas Pope and Thomas Penfold

*Chemistry- School of Natural and Environmental Sciences, Newcastle University
Newcastle upon Tyne, NE1 7RU, United Kingdom*

Contents

S1 Supplementary Results	3
S2 Model Hamiltonian	9
S3 Kinetic model	10
S4 Excitation Energy Transfer	12
S5 Fragment energy difference method	13
S6 Attachment/detachment densities	14
S7 Förster theory	15

List of Tables

S1	Electronic structure of TBPe at the geometry of minimum energy in the S_0 and S_1 states. All energies are given with respect to the energy of the optimized ground state (H : HOMO, L : LUMO).	5
S2	Electronic structure of TBPe at the geometry of minimum energy in the T_1 and T_2 states. All energies are given with respect to the energy of the optimised ground state. (H : HOMO, L : LUMO)	6
S3	Electronic structure of TBRb at the geometry of minimum energy in the S_0 and S_1 states. All energies are given with respect to the energy of the optimised ground state (H : HOMO, L : LUMO).	7
S4	Intrastate couplings κ_α of TBPe for the S_1^E and T_1^E states (in meV) incorporated in the quantum dynamics, and the frequencies of the corresponding mass-frequency weighted normal modes (in cm^{-1}). The κ_α are calculated from Eq. (S10).	10

List of Figures

S1	Excitation energy levels for the combined Au-Cz -TBPe system as a function of the separation distance (d) for the first excited singlet (left) and triplet (right) states. CT: charge transfer, LE: local excitation, CAAC: cyclic-alkyl-amino-carbene, Cz: carbazole. Energies are shown for the <i>co-planar</i> geometry.	3
S2	Strength of the EET and the Förster couplings between Au-Cz and TBPe molecules as a function of the relative orientation ($\theta_x, \theta_y, \theta_z$) for $R_{\text{DA}} = 24.2 \text{ \AA}$	4

S3	Strength of the EET and the Förster couplings between Au-Cz and TBRb molecules as a function of the relative orientation $(\theta_x, \theta_y, \theta_z)$ for $R_{DA} = 24.2 \text{ \AA}$	6
S4	Electronic density differences between excited states and the ground state with Au-Cz in the perpendicular geometry and TBRb for an intermolecular distance of $\sim 24.2 \text{ \AA}$ and a random relative orientation (blue: increase, red: decrease). The singlet and triplet states shown are those of the whole system.	8

S1 Supplementary Results

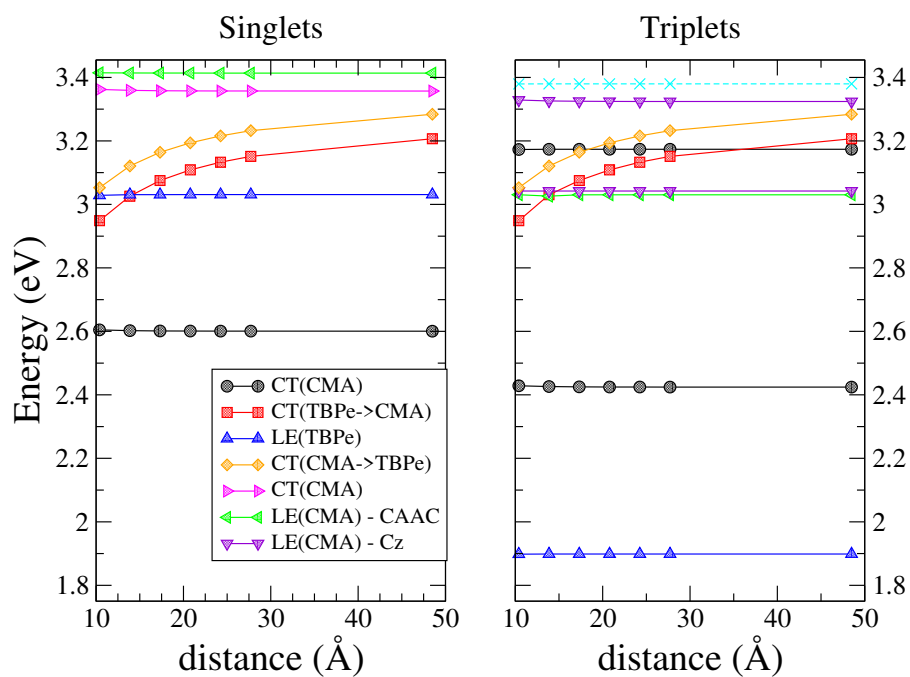


Figure S1: Excitation energy levels for the combined **Au-Cz-TBPe** system as a function of the separation distance (d) for the first excited singlet (left) and triplet (right) states. CT: charge transfer, LE: local excitation, CAAC: cyclic-alkyl-amino-carbene, Cz: carbazole. Energies are shown for the *co-planar* geometry.

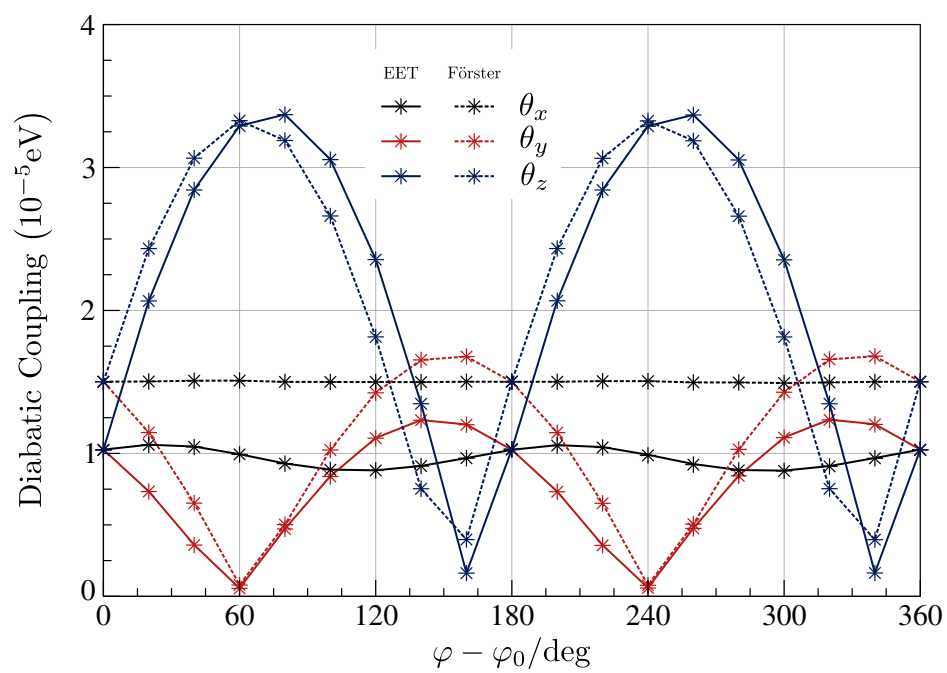


Figure S2: Strength of the EET and the Förster couplings between **Au-Cz** and TBPe molecules as a function of the relative orientation ($\theta_x, \theta_y, \theta_z$) for $R_{\text{DA}} = 24.2 \text{ \AA}$.

<i>S</i> ₀ minimum				
State	Excitation	Weight (%)	Osc. str.	Energy (eV)
<i>T</i> ₁	<i>H</i> → <i>L</i>	94.7	0.000	1.90
<i>S</i> ₁	<i>H</i> → <i>L</i>	96.4	0.662	3.03
<i>T</i> ₂	<i>H</i> - 4 → <i>L</i>	17.2	0.000	3.17
	<i>H</i> - 1 → <i>L</i>	15.1		
	<i>H</i> → <i>L</i> + 1	47.2		
	<i>H</i> → <i>L</i> + 2	16.7		
<i>T</i> ₃	<i>H</i> - 3 → <i>L</i>	54.0	0.000	3.38
	<i>H</i> → <i>L</i> + 4	37.5		
<i>S</i> ₁ minimum				
State	Excitation	Weight (%)	Osc. str.	Energy (eV)
<i>S</i> ₀	-	-	-	0.13
<i>T</i> ₁	<i>H</i> → <i>L</i>	95.7	0.000	1.53
<i>S</i> ₁	<i>H</i> → <i>L</i>	96.2	0.707	2.74
<i>T</i> ₂	<i>H</i> - 4 → <i>L</i>	24.9	0.000	2.96
	<i>H</i> - 1 → <i>L</i>	8.1		
	<i>H</i> → <i>L</i> + 1	42.0		
	<i>H</i> → <i>L</i> + 2	21.6		
<i>T</i> ₃	<i>H</i> - 3 → <i>L</i>	56.4	0.000	3.19
	<i>H</i> → <i>L</i> + 3	37.4		

Table S1: Electronic structure of TBPe at the geometry of minimum energy in the *S*₀ and *S*₁ states. All energies are given with respect to the energy of the optimized ground state (*H*: HOMO, *L*: LUMO).

T_1 minimum				
State	Excitation	Weight (%)	Osc. str.	Energy (eV)
S_0	-	-	-	0.26
T_1	$H \rightarrow L$	96.1	0.000	1.37
S_1	$H \rightarrow L$	95.9	0.736	2.63
T_2	$H - 4 \rightarrow L$	28.1	0.000	2.88
	$H - 1 \rightarrow L$	5.4		
	$H \rightarrow L + 1$	40.2		
	$H \rightarrow L + 2$	23.0		
T_3	$H - 3 \rightarrow L$	57.1	0.000	3.13
	$H \rightarrow L + 3$	37.5		

T_2 minimum				
State	Excitation	Weight (%)	Osc. str.	Energy (eV)
S_0	-	-	-	0.17
T_1	$H \rightarrow L$	94.7	0.000	1.58
S_1	$H \rightarrow L$	96.4	0.688	2.78
T_2	$H - 3 \rightarrow L$	19.2	0.000	2.84
	$H - 1 \rightarrow L$	13.6		
	$H \rightarrow L + 1$	55.9		
	$H \rightarrow L + 2$	7.9		
T_3	$H - 4 \rightarrow L$	56.2	0.000	3.30
	$H \rightarrow L + 4$	36.6		

Table S2: Electronic structure of TBPe at the geometry of minimum energy in the T_1 and T_2 states. All energies are given with respect to the energy of the optimised ground state. (H : HOMO, L : LUMO)

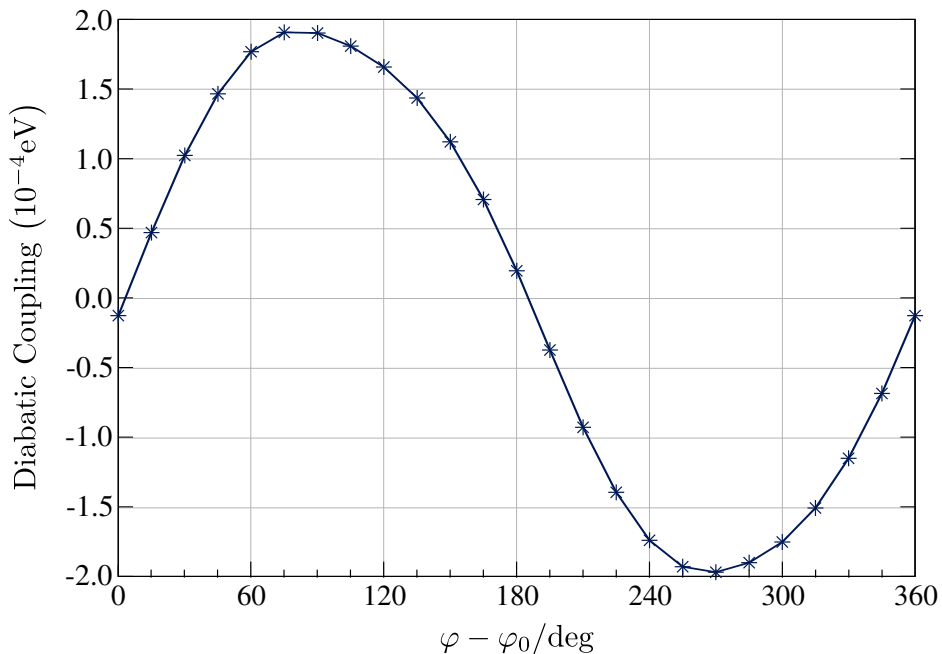


Figure S3: Strength of the EET and the Förster couplings between **Au-Cz** and TBRb molecules as a function of the relative orientation $(\theta_x, \theta_y, \theta_z)$ for $R_{\text{DA}} = 24.2 \text{ \AA}$.

<i>S</i> ₀ minimum				
State	Excitation	Weight (%)	Osc. Str.	Energy (eV)
<i>T</i> ₁	<i>H</i> → <i>L</i>	95.4	0.000	1.30
<i>S</i> ₁	<i>H</i> → <i>L</i>	95.9	0.304	2.37
<i>T</i> ₂	<i>H</i> - 1 → <i>L</i>	44.9	0.000	2.57
	<i>H</i> → <i>L</i> + 2	26.2		
	<i>H</i> - 3 → <i>L</i>	15.5		
	<i>H</i> → <i>L</i> + 6	5.1		
<i>T</i> ₃	<i>H</i> → <i>L</i> + 1	71.2	0.000	2.98
	<i>H</i> - 4 → <i>L</i>	15.3		
	<i>H</i> - 2 → <i>L</i>	8.9		
<i>S</i> ₁ minimum				
State	Excitation	Weight (%)	Osc. Str.	Energy (eV)
<i>S</i> ₀	-	-	-	0.20
<i>T</i> ₁	<i>H</i> → <i>L</i>	96.2	0.000	1.07
<i>S</i> ₁	<i>H</i> → <i>L</i>	96.2	0.359	2.16
<i>T</i> ₂	<i>H</i> - 1 → <i>L</i>	58.1	0.000	2.48
	<i>H</i> → <i>L</i> + 2	24.7		
	<i>H</i> - 3 → <i>L</i>	6.9		
<i>T</i> ₃	<i>H</i> → <i>L</i> + 1	90.1	0.000	3.00
	<i>H</i> - 4 → <i>L</i>	5.3		

Table S3: Electronic structure of TBRb at the geometry of minimum energy in the *S*₀ and *S*₁ states. All energies are given with respect to the energy of the optimised ground state (*H*: HOMO, *L*: LUMO).

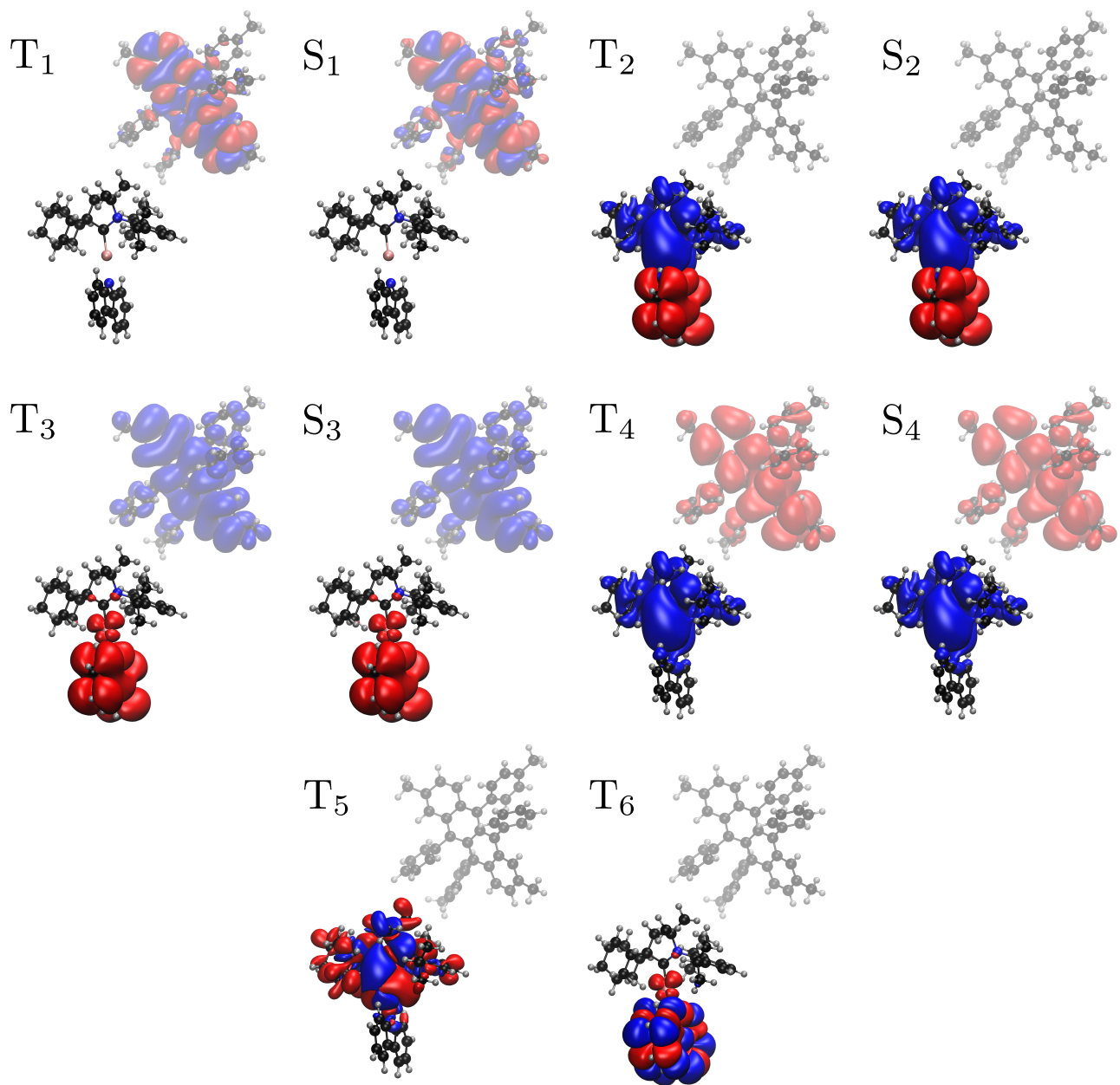


Figure S4: Electronic density differences between excited states and the ground state with **Au-Cz** in the perpendicular geometry and TBRb for an intermolecular distance of ~ 24.2 Å and a random relative orientation (blue: increase, red: decrease). The singlet and triplet states shown are those of the whole system.

S2 Model Hamiltonian

The **Au-Cz** Hamiltonian has been published elsewhere^{1,2}. The vibronic part of the TBPe Hamiltonian is written within the linear-vibronic coupling (VLC) approach³ in the diabatic picture as a function of the mass-frequency weighted normal modes \mathbf{Q} as:

$$\hat{H}_{\text{TBPe}}^{\text{vib}}(\mathbf{Q}) = \hat{T}_N(\mathbf{Q}) + \hat{W}(\mathbf{Q}), \quad (1)$$

where \hat{T}_N is the (diagonal) kinetic energy operator for the nuclei, given by:

$$\hat{T}_N(\mathbf{Q}) = -\frac{1}{2} \sum_{\alpha=1}^{3N} \omega_{\alpha} \frac{\partial^2}{\partial Q_{\alpha}^2}, \quad (2)$$

ω_{α} being the frequency of the mass-frequency weighted normal mode Q_{α} , and N the total number of atoms in the TBPe molecule. To calculate the vibronic couplings, it is convenient to expand the electronic diabatic Hamiltonian $\hat{W}(\mathbf{Q})$ around the equilibrium geometry of the ground state \mathbf{Q}_0 , assuming that the matrix elements are slowly varying functions of \mathbf{Q} :

$$\hat{W} - V_0 \mathbf{1} = \hat{W}^{(0)} + \hat{W}^{(1)} + \hat{W}^{(2)} + \dots, \quad (3)$$

where $V_0(\mathbf{Q})$ is the ground state potential energy surface:

$$V_0(\mathbf{Q}) = \frac{1}{2} \sum_{\alpha=1}^{3N} \omega_{\alpha} Q_{\alpha}^2. \quad (4)$$

In the LVC approach, the expansion is restricted to the first order, and the matrix elements become:

$$\hat{W}_{ij}^{(0)} = E_i(\mathbf{Q}_0) \delta_{ij} \quad (5)$$

$$\hat{W}_{ij}^{(1)} = V_0(\mathbf{Q}) + \sum_{\alpha=1}^{3N} \left(\frac{\partial \hat{W}_{ij}}{\partial Q_{\alpha}} \right)_{\mathbf{Q}_0} \cdot Q_{\alpha}, \quad (6)$$

where E_i are the vertical excitation energy of state i at \mathbf{Q}_0 . The vibronic coupling constants represent the \mathbf{Q} -dependent changes of the Hamiltonian due to the excitation. In this framework, we define the *intrastate* couplings as:

$$\kappa_{\alpha}^{(i)} = \left(\frac{\partial \hat{W}_{ii}}{\partial Q_{\alpha}} \right)_{\mathbf{Q}_0}, \quad (7)$$

and the *interstate* couplings as:

$$\lambda_{\alpha}^{(i,j)} = \left(\frac{\partial \hat{W}_{ij}}{\partial Q_{\alpha}} \right)_{\mathbf{Q}_0}. \quad (8)$$

The on-diagonal elements $\hat{W}_{ii}^{(1)}$, also called “tuning modes”, are responsible for structural reorganization within an excited-state potential compared to the ground state, whereas the off-diagonal elements $\hat{W}_{ij}^{(1)}$, also called “coupling modes”, are the nonadiabatic couplings responsible for transferring wavepacket population between different excited states^{3,4}.

Beside the S_1^A , T_1^A and T_2^A states of **Au-Cz**, we include the S_1^E and T_1^E states of TBPe in the Hamiltonian, giving only non-zero intrastate couplings. By construction, the adiabatic and diabatic states are identical at \mathbf{Q}_0 . The intrastate couplings are then given by:

$$\kappa_{\alpha}^{(i)} = \left(\frac{\partial V_i}{\partial Q_{\alpha}} \right)_{\mathbf{Q}_0}, \quad (9)$$

α	ω_α	$\kappa_\alpha (S_1^E)$	$\kappa_\alpha (T_1^E)$
191	1634.0	133.8	181.6
160	1437.7	130.2	172.8
141	1333.7	58.7	85.6
193	1661.7	54.0	76.6

Table S4: Intrastate couplings κ_α of TBPe for the S_1^E and T_1^E states (in meV) incorporated in the quantum dynamics, and the frequencies of the corresponding mass-frequency weighted normal modes (in cm^{-1}). The κ_α are calculated from Eq. (S10).

where V_i is the potential of the adiabatic state i . From a practical point of view, the intrastate couplings are calculating through the energy gradient at \mathbf{Q}_0 by:

$$\kappa_\alpha = \sqrt{\frac{\hbar}{\omega_\alpha}} \sum_{i=1}^{3N} \frac{1}{\sqrt{m_i}} \left(\frac{\partial q_\alpha}{\partial \zeta_i} \right)_{\mathbf{Q}_0} \left(\frac{\partial V}{\partial x_i} \right)_{\mathbf{Q}_0}, \quad (10)$$

where q_α is the normal mode α , ζ_i the mass-weighted Cartesian coordinates, x_i the Cartesian coordinates, and m_i the mass of the atom displaced by the quantity x_i . Here we include the 4 modes having the strongest couplings, which are given in table S4. Finally, we can rewrite the diagonal terms of the electronic Hamiltonian as:

$$\hat{W}_{ii} = E_i(\mathbf{Q}_0) + \sum_{\alpha=1}^{3N} \left(\frac{1}{2} \omega_\alpha Q_\alpha^2 + \kappa_\alpha^{(i)} Q_\alpha \right). \quad (11)$$

The EET coupling as a function of the torsional angle φ shown in Fig. 3.c is fitted using $\lambda(\varphi) = b \cdot \cos(\varphi - c)$ where we obtained $b = 1.47416 \times 10^{-3}$ eV and $c = 1.60478$ rad. The *sine* evolution of the coupling as a function of the torsion angle φ is similar to the interstate vibronic couplings of the **Au-Cz** molecule^{1,2}. Finally, the spin-orbit interaction between S_1^E and T_1^E is calculated in the same way as in Ref.^{1,2}.

S3 Kinetic model

The kinetics of the population of S_1^A , S_1^E , and T_1^A are described by:

$$\begin{aligned} \frac{dS_1^A(t)}{dt} &= -(k_{\text{ISC}} + k_{\text{EET}}) \cdot S_1^A(t) + k_{\text{rISC}} \cdot T_1^A(t) + k_{\text{rEET}} \cdot S_1^E(t) \\ \frac{dT_1^A(t)}{dt} &= -k_{\text{rISC}} \cdot T_1^A(t) + k_{\text{ISC}} \cdot S_1^A(t) \\ \frac{dS_1^E(t)}{dt} &= -k_{\text{rEET}} \cdot S_1^E(t) + k_{\text{EET}} \cdot S_1^A(t), \end{aligned} \quad (12)$$

where k_{ISC} is the ISC rate constant from S_1^A to T_1^A , k_{rISC} the rISC rate constant from T_1^A to S_1^A , k_{EET} the EET rate constant from S_1^A to S_1^E , and k_{rEET} the reverse EET rate constant from S_1^E to S_1^A .

The equation system in the main text can be written in a matrix formulation as:

$$\begin{pmatrix} \dot{S}_1^A(t) \\ \dot{T}_1^A(t) \\ \dot{S}_1^E(t) \end{pmatrix} = \begin{pmatrix} -(k_{\text{ISC}} + k_{\text{EET}}) & k_{\text{rISC}} & k_{\text{rEET}} \\ k_{\text{ISC}} & -k_{\text{rISC}} & 0 \\ k_{\text{EET}} & 0 & -k_{\text{rEET}} \end{pmatrix} \cdot \begin{pmatrix} S_1^A(t) \\ T_1^A(t) \\ S_1^E(t) \end{pmatrix}, \quad (13)$$

or equivalently:

$$\dot{\mathbf{P}}(t) = \hat{\mathbf{K}} \cdot \mathbf{P}(t). \quad (14)$$

If $\hat{\mathbf{K}}$ is diagonalizable, $\hat{\mathbf{K}} = \hat{\mathbf{U}}\hat{\mathbf{\Lambda}}\hat{\mathbf{U}}^{-1}$, (14) has the solution⁵:

$$\mathbf{P}(t) = e^{\hat{\mathbf{K}}t}\mathbf{P}(0) = \hat{\mathbf{U}}e^{\hat{\mathbf{\Lambda}}t}\hat{\mathbf{U}}^{-1}\mathbf{P}(0). \quad (15)$$

For clarity purposes, we use here the following notations: $a = k_{\text{ISC}}$, $b = k_{\text{rISC}}$, $c = k_{\text{EET}}$, and $d = k_{\text{rEET}}$. The rate matrix becomes:

$$\hat{\mathbf{K}} = \begin{pmatrix} -(a+c) & b & d \\ a & -b & 0 \\ c & 0 & -d \end{pmatrix}. \quad (16)$$

We further define σ_1 as the sum of the first order processes, σ_2 as the sum of some second order processes, and θ_1 as a first order combination of both:

$$\begin{aligned} \sigma_1 &= a + b + c + d \\ \sigma_2 &= ad + bc + bd \\ \theta_1 &= \sqrt{\sigma_1^2 - 4\sigma_2}. \end{aligned} \quad (17)$$

Eigenvalues of $\hat{\mathbf{K}}$ are given by:

$$\lambda_1 = 0 \quad ; \quad \lambda_2 = \frac{-(\sigma_1 + \theta_1)}{2} \quad ; \quad \lambda_3 = \frac{-(\sigma_1 - \theta_1)}{2}. \quad (18)$$

A possible eigenvectors matrix is given by:

$$\hat{\mathbf{U}} = \begin{pmatrix} \frac{d}{c} & \frac{d+\lambda_2}{c} & \frac{d+\lambda_3}{c} \\ \frac{ad}{bc} & -\left(1 + \frac{d+\lambda_2}{c}\right) & -\left(1 + \frac{d+\lambda_3}{c}\right) \\ 1 & 1 & 1 \end{pmatrix}, \quad (19)$$

and the inverse matrix by:

$$\hat{\mathbf{U}}^{-1} = \frac{1}{\sigma_2\theta_1} \begin{pmatrix} bc\theta_1 & bc\theta_1 & bc\theta_1 \\ -c(\sigma_2 + b\lambda_3) & -bc\lambda_3 & d[\sigma_2 + (a+b)\lambda_3] \\ c(\sigma_2 + b\lambda_2) & bc\lambda_2 & -d[\sigma_2 + (a+b)\lambda_2] \end{pmatrix}. \quad (20)$$

The exponential matrix is given by:

$$e^{\hat{\mathbf{K}}t} = \begin{pmatrix} 1 & 0 & 0 \\ 0 & e^{\lambda_2 t} & 0 \\ 0 & 0 & e^{\lambda_3 t} \end{pmatrix}. \quad (21)$$

The rate equations for an the initial conditions $\mathbf{P}(0) = (n, 1 - n, 0)$ is given by:

$$\begin{aligned}
S_1^A(t) &= \gamma_1 + \left[(2(b + nd) - (n + \gamma_1)\sigma_1) \frac{\sinh\left(\frac{\theta_1 t}{2}\right)}{\theta_1} + (n - \gamma_1) \cosh\left(\frac{\theta_1 t}{2}\right) \right] e^{-\sigma_1 t/2} \\
T_1^A(t) &= \gamma_2 + \left[(2(na - (1 - n)b) + (1 - n - \gamma_2)\sigma_1) \frac{\sinh\left(\frac{\theta_1 t}{2}\right)}{\theta_1} + (1 - n - \gamma_2) \cosh\left(\frac{\theta_1 t}{2}\right) \right] e^{-\sigma_1 t/2} \\
S_1^E(t) &= \gamma_3 + \left[(2nc - \gamma_3\sigma_1) \frac{\sinh\left(\frac{\theta_1 t}{2}\right)}{\theta_1} - \gamma_3 \cosh\left(\frac{\theta_1 t}{2}\right) \right] e^{-\sigma_1 t/2}, \tag{22}
\end{aligned}$$

where $\gamma_1 = \frac{bd}{\sigma_2}$, $\gamma_2 = \frac{ad}{\sigma_2}$, $\gamma_3 = \frac{bc}{\sigma_2}$.

S4 Excitation Energy Transfer

Excitation energy transfer (EET) describes the non-radiative exchange of electronic (excitonic) energy from one excited donor (D) molecule to another non-excited acceptor (A) molecule:



We are interested here in singlet EET (SEET) between the **Au-Cz-S₁** and the TPBe-S₁ states which we briefly describe. We refer the reader to Ref.⁶ for the description of triplet EET and electron transfer (ET), and for more details about singlet EET. Within the first-order approximation in the single excitation theory, the electronic coupling between D and A promoting SEET is composed of 3 parts^{7,8}:

$$V_{\text{SEET}} = V_{\text{Coul}} + V_{\text{short}} + V_{\text{solv}}, \tag{24}$$

where V_{Coul} is the coupling from the long-range Coulomb interaction between the electronic transitions, V_{short} the short-range coupling including the Dexter's coupling from the indistinguishability of electrons and the short-range coupling from the molecular orbitals overlap between D and A, and V_{solv} the explicit contribution of the solvent. The (unscreened) Coulomb interaction between the transition densities of the donor and the acceptor is given by^{7,9,10}:

$$V_{\text{Coul}} = \int \int d\mathbf{r} d\mathbf{r}' \rho_D^{\text{tr}*}(\mathbf{r}) \frac{1}{|\mathbf{r} - \mathbf{r}'|} \rho_A^{\text{tr}}(\mathbf{r}'), \tag{25}$$

where $\rho_{D/A}^{\text{tr}}$ are the transition densities of the donor and acceptor moieties. Transition densities are calculated from the diagonal part of the transition density matrices (TDM) between the ground state (0) and the excited states (I) wavefunctions:

$$\begin{aligned}
\gamma_{0I}^{\text{tr}}(\mathbf{r}, \mathbf{r}') &= N \int \cdots \int d\mathbf{r}_2 \cdots d\mathbf{r}_N \\
&\quad \times \Psi_0(\mathbf{r}, \mathbf{r}_2, \cdots, \mathbf{r}_N) \Psi_I^*(\mathbf{r}', \mathbf{r}_2, \cdots, \mathbf{r}_N) \\
\rho_{0I}^{\text{tr}}(\mathbf{r}) &= \gamma_{0I}^{\text{tr}}(\mathbf{r}, \mathbf{r}).
\end{aligned} \tag{26}$$

The total integrated transition density being zero by definition, the first nonzero term in a multipole expansion of the Coulomb coupling is the interaction of the transition dipole moments¹⁰. Transition dipole moments are given by:

$$\boldsymbol{\mu}_{0I}^{\text{tr}} = \int d\mathbf{r} \mathbf{r} \rho_{0I}^{\text{tr}}(\mathbf{r}), \tag{27}$$

and are pointing toward the positive part of the transition density.

Hsu *et al.* have developed a first-order perturbative expression within a TDDFT framework to describe the short-range coupling which is expressed as the sum of two terms:

$$V_{\text{short}} = V_{\text{xc}} + V_{\text{ovlp}}, \quad (28)$$

namely, an exchange correlation term and an overlap term, given by⁹:

$$\begin{aligned} V_{\text{xc}} &= \int \int \mathbf{d}\mathbf{r}\mathbf{d}\mathbf{r}' \rho_{\text{D}}^{\text{tr}*}(\mathbf{r}) g_{\text{xc}}(\mathbf{r}, \mathbf{r}'; \omega_0) \rho_{\text{A}}^{\text{tr}}(\mathbf{r}') \\ V_{\text{ovlp}} &= -\omega_0 \int \mathbf{d}\mathbf{r} \rho_{\text{D}}^{\text{tr}*}(\mathbf{r}) \rho_{\text{A}}^{\text{tr}}(\mathbf{r}), \end{aligned} \quad (29)$$

where g_{xc} is the exchange-correlation kernel of the selected DFT functional, and ω_0 the average resonance transition energy of D and A. Finally, within the framework of polarizable continuum models (PCM) we use here, the solvent contribution can be expressed as^{10,11}:

$$V_{\text{solv}} = \sum_k \int \mathbf{d}\mathbf{r} \rho_{\text{D}}^{\text{tr}*}(\mathbf{r}) \frac{1}{|\mathbf{r} - \mathbf{s}_k|} q_k^{\text{PCM}}(\rho_{\text{A}}^{\text{tr}}(\mathbf{r})), \quad (30)$$

which represents the interaction between the transition localized at the donor site and the PCM surface charges q^{PCM} induced by the transition localized at A, and where it has been assumed that only the electronic component of the solvent polarization is activated in the process.

S5 Fragment energy difference method

The electronic coupling in a two-state representation will be given by the off-diagonal Hamiltonian element of the diabatic states¹²:

$$V = \langle \Psi_i | \hat{H} | \Psi_f \rangle, \quad (31)$$

where Ψ_i and Ψ_f are the diabatic wave functions for the initial and final states. To construct the diabatic states, we have used the fragment energy difference (FED) method, as implemented in the QCHEM package¹³. In this approach, the diabatic states are defined as the linear combination of the D/A eigenstates that maximizes the degree of “exciton localization” through the definition of the “excitation difference” operator defined as:

$$\Delta \mathbf{x} = \begin{pmatrix} \Delta x_{11} & \Delta x_{12} \\ \Delta x_{12} & \Delta x_{22} \end{pmatrix}, \quad (32)$$

with matrix elements:

$$\Delta x_{mn} = \int_{\mathbf{r} \in \text{D}} \rho_{mn}^{\text{ex}}(\mathbf{r}) \mathbf{d}\mathbf{r} - \int_{\mathbf{r} \in \text{A}} \rho_{mn}^{\text{ex}}(\mathbf{r}) \mathbf{d}\mathbf{r}, \quad (33)$$

where ρ_{mn}^{ex} is the “excitation density”, defined as the sum of attachment (electron) and detachment (hole) densities for the transition $|m\rangle \rightarrow |n\rangle$ (see appendix E). The excitation-localized states are thus the states that diagonalize the FED matrix⁷:

$$\mathbf{U}^{-1} \begin{pmatrix} \Delta x_{11} & \Delta x_{21} \\ \Delta x_{12} & \Delta x_{22} \end{pmatrix} \mathbf{U} = \begin{pmatrix} \Delta x_i & 0 \\ 0 & \Delta x_f \end{pmatrix}, \quad (34)$$

with the unitary transformation matrix:

$$\mathbf{U} = \begin{pmatrix} \cos \theta & \sin \theta \\ -\sin \theta & \cos \theta \end{pmatrix}, \quad (35)$$

where the transformation angle θ satisfies:

$$\tan 2\theta = \frac{\Delta x_{12}}{\Delta x_{11} - \Delta x_{22}}, \quad (36)$$

which allows to write the FED coupling as⁷:

$$V_{\text{FED}} = \frac{(E_2 - E_1) |\Delta x_{12}|}{\sqrt{(\Delta x_{11} - \Delta x_{22})^2 - 4(\Delta x_{12})^2}}, \quad (37)$$

where E_1 and E_2 are the energies of the starting adiabatic states. The FED approach allows then to estimate the EET coupling given by Eq. (24).

S6 Attachment/detachment densities

In the framework of Kohn-Sham TDDFT, transition density matrix for the transition $|0\rangle \rightarrow |n\rangle$ is given as a superposition of the TDMs associated with individual single-particle transitions ($i \rightarrow a$)¹⁴:

$$\begin{aligned} \gamma_{0n}^{\text{tr}}(\mathbf{r}, \mathbf{r}') &= \sum_{i,a} \left[\phi_i(\mathbf{r}') \phi_a^*(\mathbf{r}) X_{ia}(\Omega_n) \right. \\ &\quad \left. + \phi_i^*(\mathbf{r}) \phi_a(\mathbf{r}') Y_{ia}(\Omega_n) \right], \end{aligned} \quad (38)$$

where X_{ia} and Y_{ia} are the eigenvectors of the Casida equation, Ω_n the excitation energy, and ϕ_i the KS orbitals. To calculate the attachment and detachment densities for the transition $|m\rangle \rightarrow |n\rangle$, a density difference operator is defined as¹⁵:

$$\Delta = \gamma_{0m}^{\text{tr}} - \gamma_{0n}^{\text{tr}}, \quad (39)$$

whose eigenvectors \mathbf{U} , called natural transition orbitals, are given by:

$$\mathbf{U}^\dagger \Delta \mathbf{U} = \delta, \quad (40)$$

with the eigenvalues δ_p interpreted as ‘‘occupation numbers’’. In an electronic transition which does not involve ionization or electron attachment, the sum of the occupations number will be zero. The detachment (hole) density is defined as the sum of all natural transition orbitals of the difference density with negative occupation numbers weighted by the absolute value of their occupations, and the attachment (electron) density is similarly defined from the positive occupation numbers. If we define the diagonal matrices \mathbf{d} and \mathbf{a} with elements:

$$\begin{aligned} d_p &= -\min(\delta_p, 0) \\ a_p &= \max(\delta_p, 0), \end{aligned} \quad (41)$$

the detachment density \mathbf{D} and the attachment density \mathbf{A} will be calculated from:

$$\begin{aligned} \mathbf{D} &= \mathbf{U} \mathbf{d} \mathbf{U}^\dagger \\ \mathbf{A} &= \mathbf{U} \mathbf{a} \mathbf{U}^\dagger. \end{aligned} \quad (42)$$

Finally, the difference matrix can be recalculated from:

$$\Delta = \mathbf{A} - \mathbf{D}. \quad (43)$$

See ref.¹⁵ for a detailed discussion about attachment and detachment densities.

S7 Förster theory

In the Förster theory, developed by Theodor Förster in the ~1940s^{16–18}, the electronic coupling given by Eq. (24) is approximated by V_{Coul} only, thus neglecting the short-range interactions, screened by an environmental factor determined by the inverse of the squared refractive index¹⁰ ($1/n^2$). Moreover, the Coulomb contribution is approximated by the transition dipole–transition dipole interaction. The Förster coupling is then given by:

$$V_F = \frac{V_{dd}}{n^2} = \frac{\kappa |\boldsymbol{\mu}_D| |\boldsymbol{\mu}_A|}{4\pi\epsilon_0 n^2 R_{DA}^3}, \quad (44)$$

where R_{DA} is the distance between D and A, $\boldsymbol{\mu}_{D/A}$ are the transition dipole moments, and κ the orientation factor given by:

$$\kappa = \hat{\boldsymbol{\mu}}_D \cdot \hat{\boldsymbol{\mu}}_A - 3 \left(\hat{\boldsymbol{\mu}}_D \cdot \hat{\mathbf{R}}_{DA} \right) \left(\hat{\boldsymbol{\mu}}_A \cdot \hat{\mathbf{R}}_{DA} \right), \quad (45)$$

In the weak coupling limit, as considered in the Förster theory, the rate constant is written with the Fermi golden rule (FGR):

$$k_F = \frac{2\pi}{\hbar} |V_F|^2 J, \quad (46)$$

where J is the Franck-Condon Weighted Density of States (FCWD) which ensure energy conservation, and which is written as the normalized overlap between the donor emission and acceptor absorption spectra to ensures the resonance condition during EET. By defining the Förster radius R_F as the distance at which the energy transfer efficiency is 50%, and τ_D as the fluorescence lifetime of the donor in the absence of the acceptor, it is possible to show that the Förster rate constant can be rewritten¹⁹:

$$k_F = \left(\frac{R_F}{R_{DA}} \right)^6 \frac{1}{\tau_D}, \quad (47)$$

which we have used to fit the data from quantum dynamics to estimate the Förster radius.

References

- [1] S. Thompson, J. Eng and T. Penfold, *The Journal of chemical physics*, 2018, **149**, 014304.
- [2] J. Eng, S. Thompson, H. Goodwin, D. Credginton and T. J. Penfold, *Physical Chemistry Chemical Physics*, 2020, **22**, 4659–4667.
- [3] T. J. Penfold, E. Gindensperger, C. Daniel and C. M. Marian, *Chemical reviews*, 2018, **118**, 6975–7025.
- [4] H. Köppel, W. Domcke and L. S. Cederbaum, *Advances in Chemical Physics*, 1984, 59–246.
- [5] G. Strang, *Linear algebra and its applications*, Academic press, 2014.
- [6] C.-P. Hsu, *Accounts of Chemical Research*, 2009, **42**, 509–518.
- [7] Z.-Q. You and C.-P. Hsu, *International Journal of Quantum Chemistry*, 2014, **114**, 102–115.
- [8] C. Azarias, R. Russo, L. Cupellini, B. Mennucci and D. Jacquemin, *Physical Chemistry Chemical Physics*, 2017, **19**, 6443–6453.
- [9] C.-P. Hsu, G. R. Fleming, M. Head-Gordon and T. Head-Gordon, *The Journal of Chemical Physics*, 2001, **114**, 3065–3072.

- [10] L. Cupellini, M. Corbella, B. Mennucci and C. Curutchet, *Wiley Interdisciplinary Reviews: Computational Molecular Science*, 2019, **9**, e1392.
- [11] M. F. Iozzi, B. Mennucci, J. Tomasi and R. Cammi, *The Journal of chemical physics*, 2004, **120**, 7029–7040.
- [12] K. Y. Kue, G. C. Claudio and C.-P. Hsu, *Journal of chemical theory and computation*, 2018, **14**, 1304–1310.
- [13] C.-P. Hsu, Z.-Q. You and H.-C. Chen, *The Journal of Physical Chemistry C*, 2008, **112**, 1204–1212.
- [14] F. Furche, *The Journal of Chemical Physics*, 2001, **114**, 5982–5992.
- [15] M. Head-Gordon, A. M. Grana, D. Maurice and C. A. White, *The Journal of Physical Chemistry*, 1995, **99**, 14261–14270.
- [16] T. Förster, *Naturwissenschaften*, 1946, **33**, 166–175.
- [17] T. Förster, *Ann. Phys*, 1948, **2**, 55.
- [18] T. Förster, *Journal of biomedical optics*, 2012, **17**, 011002.
- [19] T. Förster, *Discussions of the Faraday Society*, 1959, **27**, 7–17.